NMDAR-activated PP1 dephosphorylates GluN2B to modulate NMDAR plasticity.

Andrew M. Chiu[1], Jiejie Wang[1,2], Michael P. Fiske[3], Pavla Hubalkova[1,4], Levi Barse[1], John A. Gray[5], and Antonio Sanz-Clemente[1*].

[1] Department of Pharmacology, Feinberg School of Medicine, Northwestern University. Chicago, IL
[2] Department of Neurology, University of California, San Francisco. San Francisco, CA
[3] Department of Physiology, Feinberg School of Medicine, Northwestern University, Chicago, IL
[4] Department of Cellular Neurophysiology, Institute of Physiology CAS. Prague, Czech Republic
[5] Department of Neurology, Center for Neuroscience, University of California, Davis. Davis, CA

* Corresponding author: Antonio Sanz-Clemente Ph.D.
Department of Pharmacology
Northwestern University. Feinberg School of Medicine
Chicago, IL. 60611
antonio.sanz-clemente@northwestern.edu

Number of Figures: 4
Number of Words in summary: 144
Number of Words: 6,813

Summary
In mature neurons, postsynaptic NMDARs are segregated in two populations, synaptic and extrasynaptic NMDARs, which differ in localization, function and associated intracellular cascades. These two pools are connected via lateral diffusion, and receptor exchange between them modulates synaptic NMDAR content (NMDAR-plasticity). Here, we identify the phosphorylation of the PDZ-ligand of the GluN2B subunit of NMDARs (at S1480) as a critical determinant in dynamically controlling NMDAR subsynaptic localization. We find that this phosphorylation maintains NMDARs segregated at extrasynaptic membranes as part of a protein complex containing inactive Protein Phosphatase 1 (PP1). Global (synaptic and extrasynaptic) activation of NMDARs lead to the activation of PP1, which mediates dephosphorylation of GluN2B at S1480 and promotes an increase in synaptic NMDAR content. Thus, PP1-mediated dephosphorylation of the PDZ-ligand of GluN2B contributes to NMDAR-plasticity regulation, a process with profound consequences for synaptic and structural plasticity, metaplasticity, and synaptic neurotransmission.

Introduction

N-methyl-D-Aspartate receptors (NMDARs) are ionotropic glutamate receptors essential for excitatory neurotransmission in the brain (Paoletti et al., 2013). In mature neurons, functional postsynaptic NMDARs are segregated in two different locations: synaptic NMDARs, which are encapsulated within the postsynaptic density (PSD), and extrasynaptic NMDARs, which are associated with extrasynaptic membranes (Papouin and Oliet, 2014). These two populations have distinct functions and trigger different intracellular cascades. For example, synaptic NMDAR activation induces classical forms of synaptic plasticity (i.e., LTP and LTD) and activates ERK and CREB signaling, whereas extrasynaptic NMDARs have neuronal modulatory roles and inhibit ERK and CREB pathways (Papouin and Oliet, 2014; Parsons and Raymond, 2014). The NMDAR content in these populations is plastic and can be dynamically modified in response to different stimuli (Paoletti et al., 2013; Sanz-Clemente et al., 2013b). The paradigmatic example is the switch in the synaptic GluN2 subunit composition of NMDARs that occurs at early developmental stages (from predominantly GluN2B-containing to predominantly GluN2A-containing NMDARs) which decisively contributes to synaptic maturation (Sanz-Clemente et al., 2013b). Growing evidence shows that synaptic NMDARs are subject to activity-dependent regulation in mature neurons as well. Indeed, there have been protocols described to induce both increases and decreases in synaptic NMDAR content (NMDAR-LTP and -LTD) (Hunt and Castillo, 2012). This bidirectional NMDAR-plasticity has been hypothesized to affect important synaptic functions such as metaplasticity and homeostatic plasticity, and to modify the integrative properties of the neuron (Dore et al., 2017; Hunt and Castillo, 2012). Mechanistically, both an increase in surface-expressed NMDARs and the synaptic recruitment of extrasynaptic NMDARs contributes to NMDAR-LTP (Harney et al., 2008; Tovar and Westbrook, 2002). However, the molecular determinants controlling these processes are not fully understood.

We have previously identified a molecular mechanism controlling the clearance of GluN2B-containing NMDARs from synaptic sites. Briefly, we have shown that the activity-dependent phosphorylation of the PDZ-ligand of GluN2B (on S1480; GluN2B-pS1480) disrupts the interaction of NMDARs with scaffolding proteins such as PSD-95 and promotes the lateral diffusion of the receptors to extrasynaptic sites (Chen et al., 2012; Sanz-Clemente et al., 2013a; Sanz-Clemente et al., 2010). We report here that phosphorylation of GluN2B on S1480 is not permissive for NMDAR bidirectional exchange between synaptic and extrasynaptic populations, but it restricts the receptors to extrasynaptic membranes. Therefore, GluN2B-containing NMDARs have to be dephosphorylated in order to re-enter into synaptic sites. We have identified Protein Phosphatase 1 (PP1) as the phosphatase mediating this reaction. Additionally, we have outlined the molecular determinants that control this process by showing that extrasynaptic NMDARs form a protein complex containing inactive PP1. Global activation of NMDARs leads to the activation of PP1, which induces dephosphorylation of GluN2B-pS1480 and promotes the reinsertion of extrasynaptic GluN2B receptors into the PSDs. This novel mechanism, therefore, controls NMDAR-plasticity in mature neurons by regulating synaptic/extrasynaptic NMDAR balance.

Results

We have previously identified a molecular mechanism promoting the clearance of GluN2B-containing NMDARs from the PSDs, which is based on the synaptic activity-dependent phosphorylation of the GluN2B subunit within its PDZ-ligand domain (on S1480; GluN2B-pS1480). Briefly, GluN2B-pS1480 disrupts the interaction of NMDARs with synaptic scaffolding proteins (e.g., PSD-95), which facilitates lateral diffusion to extrasynaptic sites, where the phosphorylated receptor is internalized in a clathrin-dependent manner (Chen et al., 2012; Sanz-Clemente et al., 2013a; Sanz-Clemente et al., 2010). Because GluN2B-containing NMDARs are fated for recycling (Lavezzari et al., 2004) and GluN2B-pS1480 seems to be permissive for lateral diffusion between synaptic and extrasynaptic populations, we initially hypothesized that internalized NMDARs would be recycled and reinserted into the PSD. This idea would be consistent with recent work using single molecule tracking which demonstrated that GluN2B-containing NMDARs exchange between synaptic and extrasynaptic populations via lateral diffusion (Dupuis et al., 2014).

We first tested this hypothesis by using an antibody feeding approach in primary hippocampal neurons overexpressing GFP-GluN2B wild-type (WT) or the phospho-mimetic mutant GluN2B S1480E. Consistent with our hypothesis, we found that the phosphomimetic mutant was readily recycled to the plasma membrane to a level comparable to GluN2B WT (Figure 1A). Next, as a first step to test the reinsertion of phosphorylated receptors to the PSD, we evaluated NMDAR surface and synaptic expression by conducting genetic molecular replacement experiments in floxed GluN2A/2B mice as previously described (Chen et al., 2012; Sanz-Clemente et al., 2013a). Briefly, we used organotypic hippocampal slices biolistically co-transfected with either Cre alone, to remove endogenous GluN2A and GluN2B, or Cre with exogenous GluN2B S1480E. After allowing for enough time for steady state receptor expression, we measured both evoked NMDAR-mediated synaptic currents (NMDAR-EPSCs) and whole cell responses to puffed-on NMDA. As we have previously shown (Chen et al., 2012), we found that neurons expressing only the phosphomimetic mutant GluN2B S1480E lacked any elicitable NMDAR-EPSCs (Figure 1B). However, consistent with our previous imaging data (Sanz-Clemente et al., 2010), we found that whole cell responses were present in neurons expressing GluN2B S1480E (Figure 1C).

These data indicate that, while a population of phosphorylated receptors can be trafficked to the surface, these receptors are excluded from the PSDs and restricted to extrasynaptic sites. These findings suggest that GluN2B-pS1480 is not permissive for free bidirectional lateral diffusion and indicate that the NMDAR lateral diffusion from and to synaptic sites is controlled by distinct molecular mechanisms. Based on these data, we formulated our central hypothesis: surface expressed GluN2B-containing NMDARs must be dephosphorylated in the GluN2B PDZ-ligand before being integrated into the PSD.

Global activation of NMDARs promote Protein Phosphatase 1 (PP1)-mediated dephosphorylation of S1480 at surface-expressed GluN2B subunits.

If GluN2B needs to be dephosphorylated to re-enter at PSDs, then GluN2B S1480 has to be bidirectionally regulated, and dephosphorylation should occur at surface-expressed GluN2B-containing NMDARs. To test our hypothesis, we first induced GluN2B dephosphorylation in

primary cortical cultures by globally activating NMDARs as previously described (bath application of 50 μM NMDA for 10 min) (Chung et al., 2004). Next, we isolated surface-expressed NMDARs using two independent methods, biotinylation (Figure 2A) and biochemical isolation of the synaptic plasma membranes (SPM) (Figure 2B). Finally, we quantified the levels of GluN2B-pS1480 by immunoblotting using a custom-generated antibody against the phosphorylated state of GluN2B on S1480 (Figure S1). As expected, global activation of NMDAR promoted a robust dephosphorylation of GluN2B-pS1480 in whole cell lysate. In both experiments, we observed a similar reduction on surface-expressed GluN2B indicating that global NMDAR activation dephosphorylates the NMDAR population with the potential to be integrated into the PSD through lateral insertion.

Because previous studies have shown that synaptic NMDAR activation induces GluN2B-pS1480 and global NMDAR activation promotes dephosphorylation (Chung et al., 2004; Sanz-Clemente et al., 2010) (Figures 2A/B), we wondered if selective activation of extrasynaptic NMDARs would be sufficient for GluN2B-pS1480 dephosphorylation. Thus, we utilized an established protocol for the preferential stimulation of extrasynaptic NMDARs in primary cortical cultures (Hardingham et al., 2002). Briefly, we inhibited synaptic NMDARs by promoting their opening (by incubating with bicuculline) in the presence of the irreversible NMDAR blocker MK-801. After MK-801 withdrawal, remaining functional NMDARs (i.e., mostly extrasynaptic) were activated by bath application of NMDA as before. The level of phosphorylated CREB was evaluated as a control. This protocol was unable to maximally dephosphorylate GluN2B-pS1480 (Figures 2C), suggesting that both synaptic and extrasynaptic NMDAR population contribute to GluN2B dephosphorylation.

We finally sought to identify the phosphatase directly responsible for this reaction. Because the majority of dephosphorylation reactions are controlled by the phosphoprotein phosphatase family (Virshup and Shenolikar, 2009), we first used a pharmacologic approach to inhibit members of this family in neuronal cultures and probed for changes in the baseline of GluN2B-pS1480. As shown in Figure 2D, we observed a robust increase in GluN2B-pS1480 in neurons treated with okadaic acid (OA, 50 nM) and calyculin A (Cal A, 100 nM). At the concentrations used, both these inhibitors block protein phosphatase 1 (PP1) and protein phosphatase 2A (PP2A). Because treatment with fostriecin, a PP2A and PP4 inhibitor, was unable to cause changes in GluN2B S1480 phosphorylation, we hypothesized that PP1 is the phosphatase responsible for GluN2B-pS1480 dephosphorylation. Supporting this idea, the incubation of cultured neurons with low concentrations of OA (under 50 nM) which preferentially inhibits PP2A (Ishihara et al., 1989), was unable to modulate GluN2B S1480 phosphorylation levels (Figure 2D). Importantly, pre-incubation with Cal A (Figure 2E) or 50 nM OA (not shown) blocked the NMDA-triggered dephosphorylation of GluN2B-pS1480 demonstrating that PP1 also controls the agonist-driven reaction. We confirmed the involvement of PP1 in GluN2B-pS1480 dephosphorylation by using a genetic approach and generated lentiviruses expressing the two isoforms of PP1 present in dendrites, PP1α and PP1γ1 fused to GFP (Strack et al., 1999). We infected cultured neurons with GFP-only or the dominant negative form D95N (Zhang et al., 1996) for 7-10 days and tested the levels of GluN2B-pS1480 by immunoblotting. As expected, overexpression of nonfunctional PP1 prevents NMDA-driven dephosphorylation of GluN2B S1480 in neurons, supporting that PP1 is the phosphatase responsible for GluN2B-pS1480 dephosphorylation (Figure 2F).

Together, our data demonstrate that global activation of NMDARs triggers the PP1-mediated dephosphorylation of GluN2B-pS1480 on NMDARs expressed at the cell surface.

Regulation of the PP1-dependent dephosphorylation of GluN2B S1480

PP1 is a constitutively active phosphatase with little inherent specificity. Thus, the cell utilizes several molecular mechanisms to regulate PP1 activity (Figure 3A) (Cohen, 2002). These include (1) direct inhibitory phosphorylation of the PP1 c-terminus, a reaction canonically controlled by CDK5, (2) complexing with inhibitor proteins to block accessibility to the active site, and (3) complexing of active PP1 with target specifying proteins to confer specificity and restrict PP1 to a specific subcellular compartment (Figure 3A). Next, we sought to examine which of these modes of PP1 regulation participate in GluN2B-pS1480 dephosphorylation.

CDK5-mediated phosphorylation of PP1 (at T320) inhibits phosphatase activity by blocking the access of PP1 to its substrates. As previously reported (Hou et al., 2013), we found that bath application of NMDA to primary neuronal cultures causes a global reduction in PP1 T320 phosphorylation (i.e., increasing the amount of active PP1) (Figure S2A).

Cells express several inhibitor proteins which complex with PP1 to block access to the active site, including inhibitor 1 (I-1), inhibitor-2 (I-2), and dopamine- and cAMP-regulated phosphoprotein-32 (DARPP-32). In turn, these inhibitors are regulated by kinase and phosphatase activity to allow for signal integration (Eto and Brautigan, 2012). The involvement of I-1 and DARPP-32 in GluN2B-pS1480 regulation is unlikely because of their relatively low expression in hippocampal CA1 neurons (Glausier et al., 2010). Nevertheless, pharmacological manipulations in culture to modulate I-1 and DARPP-32 activation failed in controlling GluN2B-pS1480 dephosphorylation, excluding them as a molecular players in this process (Figures S2B-D). We next tested the involvement of Inhibitor 2 (I-2), which functions as an active inhibitor in its dephosphorylated state (Siddoway et al., 2013). Phosphorylation of I-2 by GSK3β inactivates the inhibitor and global NMDAR activation causes both an increase in active GSK3β and an increase in phosphorylated I-2 (Szatmari et al., 2005). I-2, therefore, is an appealing candidate for PP1 inhibition in our reaction. As before, we used a pharmacological approach and inhibited GSK3β in neuronal cultures using the GSK3 specific inhibitor CHIR99021 (10 μM for 2 hours). GSK3β blockade prevented the NMDA-mediated GluN2B-pS1480 dephosphorylation, suggesting a role for I-2 in this process (Figures 3B).

The last key piece of PP1 regulation is correct targeting and complexing of PP1 with its substrate. To achieve spatial specificity, the cell expresses a large number of target specifying proteins which function to complex PP1 with a substrate in a specific subcellular compartment (Hendrickx et al., 2009). Because PP1 is canonically thought of as a cytosolic protein, but dephosphorylation occurs on surface-expressed NMDARs (Figure 2A/B), we hypothesized that PP1 might translocate to a plasma membrane-associated population in response to NMDAR activation. To examine this possibility, we first utilized Total Internal Reflection Fluorescence (TIRF) microscopy in primary hippocampal cultures. This imaging technique enables examination of dynamic processes that occur within 100 nm of the plasma membrane. We overexpressed GFP-PP1 in hippocampal neurons and tracked its targeting to the surface in response to NMDA treatment over time. As a control, we used GFP-CaMKII, as the translocation of this kinase to the synapses after NMDAR

activation has been extensively characterized (Merrill et al., 2005). As expected, CaMKII showed robust surface trafficking in response to NMDA treatment but, surprisingly, PP1 showed no change in surface levels (Figure 3C). Because overexpression of GFP-PP1 may saturate the system, we next isolated the SPM fraction following NMDA treatment in primary cortical neurons and quantified the levels of endogenous PP1 associated with SPM by immunoblotting (Figures 3D). Again, we observed a strong enrichment of CaMKII in the SPM fraction after NMDA treatment, with no increase in SPM-associated PP1. These data indicate that the PP1 population responsible for GluN2B S1480 dephosphorylation is present at the plasma membrane, likely, already associated with NMDARs. To test this possibility, we isolated GluN2B-containing protein complexes from extrasynaptic membranes from adult rat brain performing co-immunoprecipitation experiments. We solubilized SPM fraction with 1% Triton X-100 and, after centrifugation at 100,000g, we incubated the supernatant with a specific GluN2B antibody. As shown in Figure 3E, both PP1 and I-2 co-immunoprecipitated with GluN2B, demonstrating that they are part of the same protein complex.

Together, our results demonstrate that extrasynaptic GluN2B-containing NMDARs interacts with inactive PP1 and I-2. NMDAR activation leads to the activation of PP1 and dephosphorylation of GluN2B-pS1480.

GluN2B-pS1480 dephosphorylation is developmentally regulated.

We have previously demonstrated that the phosphorylation of GluN2B-pS1480 is developmentally regulated, as it peaks during the second postnatal week, the period for the synaptic GluN2 subunit switch (Sanz-Clemente et al., 2010). We investigated if the dephosphorylation reaction is also developmentally controlled by inducing NMDA-dependent GluN2B-pS1480 dephosphorylation in primary cortical neurons at different developmental stages (from DIV7 to DIV28-29). We found a strong influence of age in the dephosphorylation process: in immature neurons (DIV7), NMDA treatment promoted a small increase in GluN2B-pS1480, rather than the expected decrease that we observed from DIV14, and this response was potentiated with age (Figure 3F).

We next investigated the mechanism underlying this age dependency and found the levels of PP1 associated with SPMs are strongly developmentally regulated (Figure 3G). Low amounts of PP1 were detectable in the SPM fraction isolated from immature mouse brain (P7) whereas PP1 surface expression dramatically increased throughout brain maturation. This is not a mere consequence of changes in PP1 total expression, as PP1 is strongly expressed since early development (Figure 3G). Therefore, our data strongly suggest that the influence of development in the GluN2B-pS1480 dephosphorylation reaction is mediated by strict spatiotemporal regulation of PP1 expression.

PP1 activity modulates NMDAR synaptic localization.

If our hypothesis that GluN2B-pS1480 restricts NMDARs to extrasynaptic membranes is correct, then modulation of PP1 activity against GluN2B S1480 should cause changes in both synaptic signaling and synaptic GluN2B receptor content (Figure 4A). To test this idea, we first examined changes in ERK phosphorylation, a stereotypic event coupled to synaptic NMDAR activation. We modulated GluN2B-pS1480 in cultured neurons with NMDA (50 μM for 10 min) or OA (50 nM for 45 min) and, after drug withdrawal, we increased synaptic activity in the culture using a

standard pharmacological approach [20 μM bicuculline and 100 μM 4-AP incubation (Bic/4-AP)]. As expected, cells treated with Bic/4-AP showed a robust increase in ERK phosphorylation that, consistent with our hypothesis, was potentiated in neurons pre-treated with NMDA. Conversely, cells pre-treated with OA to block PP1 activity displayed a reduced increase in ERK phosphorylation after Bic/4-AP treatment in comparison with control cells (please, note the expected elevated basal ERK phosphorylation in OA pre-treated neurons in comparison with controls) (Figure 4B).

We next employed super-resolution microscopy in primary hippocampal cultures after transfection of GFP-GluN2B. Specifically, we quantified receptor synaptic expression, defined as the colocalization index with endogenous PSD-95, after pharmacological treatment using Structured Illumination Microscopy (SIM) (Figure 4C). Incubation with NMDA to promote GluN2B-pS1480 dephosphorylation increased the synaptic expression of GFP-GluN2B, whereas OA treatment, which enhances GluN2B-pS1480, decreased GluN2B synaptic content (Figure 4D).

To confirm these data in a more intact preparation, we employed ex vivo PP1 manipulation in acute hippocampal slices. Slices treated with NMDA induced dephosphorylation of GluN2B S1480. Concurrent with this change in phosphorylation, we observed a robust increase in the normalized synaptic GluN2B content. Conversely, slices treated with calyculin A, the most effective PP1 inhibitor in acute slices, displayed an increase in GluN2B-pS1480 and a concomitant decrease in GluN2B synaptic content (Figure 4D). Together, we these data strongly support the idea that PP1 is a crucial regulator of GluN2B-containing NMDAR trafficking and controls synaptic NMDAR content (Figure 4E).

Discussion

In this study, we identify the PP1-mediated dephosphorylation of the PDZ-ligand of GluN2B (at S1480) as a critical determinant for controlling NMDAR-plasticity. Specifically, we show that phosphorylated NMDARs are restricted at extrasynaptic membranes complexing with inhibited PP1. Global activation of NMDARs results in PP1 activation and dephosphorylation of GluN2B. Our data support a model in which dephosphorylated receptors are reintegrated into the PSDs to modulate NMDAR synaptic content. Our observations indicate that GluN2B-pS1480 is not a molecular event that allows permissive bidirectional exchange between synaptic and extrasynaptic NMDARs, but reinsertion into the PSDs requires the regulated dephosphorylation of GluN2B-pS1480. This mechanism is selective for GluN2B-containing NMDARs as GluN2A PDZ-ligand is not efficiently phosphorylated by CK2 (Sanz-Clemente et al., 2010).

Our findings expand our previous work characterizing the molecular events controlling the synaptic activity-dependent phosphorylation of the PDZ-ligand of GluN2B (Lussier et al., 2015). Briefly, we showed that casein kinase 2 (CK2) phosphorylates GluN2B S1480 after being complexed with synaptic NMDARs via activated CaMKII (Sanz-Clemente et al., 2013a). GluN2B-pS1480 disrupts the PDZ-mediated interaction of NMDARs with MAGUK proteins to promote NMDAR clearance from the synaptic sites and internalization of the receptors (Chung et al., 2004; Sanz-Clemente et al., 2010). We have now identified the mechanism underlying the reinsertion of recycled receptors to the PSDs. Together, our data show that the dynamic regulation of the phosphorylated state of the PDZ-ligand of GluN2B is a key modulator of NMDAR-plasticity, a term that refers to the activity-dependent modifications in the level of synaptic NMDARs. Both NMDAR-LTP and –LTD have been observed in several brain areas, often after stimulation with physiologically-relevant protocols of induction (Dore et al., 2017; Hunt and Castillo, 2012). Given the essential functional and regulatory roles displayed by synaptic NMDARs, NMDAR-plasticity has emerged as a key mechanism for controlling neuronal function. The most evident consequence of NMDAR-plasticity is the modulation of metaplasticity by modifying the induction threshold of AMPAR-plasticity. However, other neuronal properties as the integration of synaptic inputs or the control of homeostatic plasticity may also be affected (Dore et al., 2017; Hunt and Castillo, 2012). The precise molecular mechanisms underlying NMDAR-plasticity remain unclear, although the co-activation of NMDARs and GPCRs (i.e., mGluR1/5 or mAChRs) have been reported (Dore et al., 2017). Here, we identify a molecular mechanism that controls the synaptic recruitment of extrasynaptic NMDARs to synaptic sites, a process previously identified to contribute to NMDAR-plasticity (Dupuis et al., 2014; Harney et al., 2008). Regulation of synaptic/extrasynaptic NMDAR exchange is important because elevated extrasynaptic NMDAR signaling triggers excitotoxicity and alterations in the NMDAR balance has been associated with several neurological disorders including Huntington's disease, traumatic brain injury (TBI), and epilepsy (Parsons and Raymond, 2014). Therefore, impairments in the PP1-mediated regulation of NMDAR-plasticity may contribute to the pathophysiology of these disorders.

PP1 is a ubiquitously expressed serine/threonine phosphatase, although in neurons, it is enriched in dendritic spines (Strack et al., 1999). Our finding that activation of PP1 induces NMDAR-LTP by dephosphorylating GluN2B PDZ-ligand is unexpected as phosphatases, and particularly PP1, have been associated with the depression of synaptic activity rather than its potentiation (Woolfrey and Dell'Acqua, 2015). In fact, compelling evidence supports a model in which PP1 induces

AMPAR-LTD by dephosphorylating the GluA1 subunit of AMPAR (at S845) and CaMKII (at T256) (Siddoway et al., 2014). Although it can occur independently, NMDAR-plasticity is often coinduced with AMPAR-plasticity (Hunt et al., 2013). How, then, can PP1 activity drive opposite effects in NMDARs and AMPARs (i.e., NMDAR-LTP versus AMPAR-LTD)? We propose that PP1 subsynaptic localization is a critical factor for the different outcomes. Therefore, the stimuli classically used to induce AMPAR-LTD would activate synaptic resident-PP1 but not the PP1 pool associated with GluN2B at the extrasynaptic membranes (as extrasynaptic NMDARs would not be activated). Conversely, strong stimuli required for the induction of NMDAR-LTP would cause a robust release of glutamate, enough to spillover and activate both synaptic and extrasynaptic NMDARs. This would result in the induction of both AMPAR-LTP (by CaMKII activation and AMPAR phosphorylation) and NMDAR-LTP (by PP1 activation and dephosphorylation of GluN2B-pS1480). The existence of different subsynaptic pools of PP1 that can be differentially activated is supported by the fact the stimulus used to induce AMPA-LTD in culture recruits PP1 to the synaptic sites (Morishita et al., 2001), whereas our biochemical and TIRF data indicates that global NMDAR activation does not. In summary, our data reveal a critical role for PP1 in controlling NMDAR-plasticity by mediating the dephosphorylation of GluN2B upon global activation of NMDARs.

Materials and Methods

Neuronal Cultures, Acute Slices, Animals, Antibodies, and Reagents

Primary neuronal cultures were generated from E18 Sprague-Dawley rats as previously described (Roche and Huganir, 1995). The care and use of animals were in accordance to the guidelines set by the Northwestern IACUC. For biochemical experiments, primary cortical neuronal cultures were used due to the ease of generating enough material for analysis. For imaging-based experiments, hippocampal primary neuronal cultures were utilized.

Acute cortical slices were generated from adult (8-14 week) C57/B6 mice. Mice were anesthetized with isoflurane prior to decapitation. Coronal slices (300 µM thick) were cut in ice-cold artificial cerebrospinal fluid containing the following composition (in mM): NaCl 130, KCl 3.5, Glucose 10, NaH_2PO_4 1.25, $NaHCO_3$ 24, $CaCl_2$ 1, $MgCl_2$ 2. The slices were incubated for 30 min at 30-32°c and allowed to rest for at least 1 hour at room temperature in normal ACSF containing (in mM): NaCl 130, KCl 3.5, Glucose 10, NaH_2PO_4 1.25, $NaHCO_3$ 24, $CaCl_2$ 2, $MgCl_2$ 1. For biochemical experiments, slices were incubated at 32°C in normal ACSF or calcium-free ACSF (calcium was replaced by 2 mM EGTA). Following pharmacologic manipulation, slices were flash frozen and subject to subsequent lysis or fractionation.

Antibodies against phosphorylation state-specific GluN2B S1480 were generated by New England Peptide. Antibodies against GluN2B and PSD-95 were obtained from Neuromab. Transferrin, CaMKII, and PP1γ were obtained from Thermo Fisher. PP1 antibody was obtained from Santa Cruz. All drugs and inhibitors were obtained from Tocris biosciences.

Viruses were generated by transfecting Lenti-X cells (Clontech) with psPAX2, pMD2.G, and the pLVX backbone containing the indicated construct. The viral supernatant was harvested 72 hours post transfection and concentrated using polyethylene glycol for 24 hours. Concentrated virus was resuspended 100x in PBS and stored at -80ºC until use.

Electrophysiology in Organotypic Slice Cultures

Double-floxed GluN2A/GluN2B (*Grin2a*$^{fl/fl}$*Grin2b*$^{fl/fl}$) mice were generated as previously described (Akashi et al., 2009; Gray et al., 2011; Mishina and Sakimura, 2007). Cultured slices were prepared and transfected as previously described (Schnell et al., 2002). Briefly, hippocampi were dissected from P7 *Grin2a*$^{fl/fl}$*Grin2b*$^{fl/fl}$ mice and biolistically co-transfected after 2-4 days in culture with pFUGW-Cre:mCherry (expressing a nuclear targeted Cre:mCherry fusion protein) and either pCAGGS-GFP or pCAGGS-GluN2B-S1480E-IRES-GFP. Slices were cultured for an additional 14–20 days before recording. Slices were recorded in a submersion chamber on an upright Olympus microscope, perfused in room temperature normal ACSF saturated with 95% O2/5% CO2. Picrotoxin (0.1 mM) and NBQX (10 µM) were added to the ACSF to block GABAA and AMPA receptors respectively. CA1 pyramidal cells were visualized by infrared differential interference contrast microscopy and transfected neurons were identified by epifluorescence microscopy. The intracellular solution contained (in mM) $CsMeSO_4$ 135, NaCl 8, HEPES 10, Na-GTP 0.3, Mg-ATP 4, EGTA 0.3, and QX-314 5. Cells were recorded with 3 to 5MΩ borosilicate glass pipettes, following stimulation of Schaffer collaterals with bipolar electrodes placed in

stratum radiatum of the CA1 region. Series resistance was monitored and not compensated, and cells in which series resistance varied by 25% during a recording session were discarded. Synaptic responses were collected with a Multiclamp 700B amplifier (Axon Instruments, Foster City, CA), filtered at 2 kHz, digitized at 10 Hz. All paired recordings involved simultaneous whole-cell recordings from transfected neuron and a neighboring untransfected neuron. NMDAR-EPSCs were recorded at +40 mV in the presence of 10 μM NBQX. The stimulus was adjusted to evoke a measurable, monosynaptic EPSC in both cells. Whole cell NMDA responses were evoked with 100 μM NMDA (in ACSF) pressure-ejected (puffed) from a glass pipette by a Picospritzer III (Parker-Hannifin, Hollis, NH). Slices were aligned such that NMDA was puffed over the soma of the cell pair and perfused along the apical dendrites following the bath flow direction. Paired amplitude data were analyzed with a Wilcoxon signed-rank test and comparison of paired data groups were performed using a Mann-Whitney U test. Linear regressions were obtained using the least-squares method. All errors bars represent standard error measurement (SEM).

Immunofluorescence

Receptor surface expression was analyzed as previously described (Sanz-Clemente et al., 2010). Briefly, hippocampal neurons were transfected at DIV7 with GFP-tagged GluN2B (WT or mutants), and surface-expressed receptors were labeled with anti-GFP antibody for 15 min at RT at DIV11–12. Following internalization receptors, remaining surface receptors were blocked with Fab. After allowing for recycling of receptors back to the surface, cells were washed and fixed with 4% PFA in PBS containing 4% sucrose. Surface cells were labeled with Alexa 555-conjugated secondary antibody (shown in white for clarity). The intracellular pool of receptors was identified by permeabilizing cells with 0.25% TX-100 and labeling anti-GFP tagged receptors with Alexa 633-conjugated secondary antibodies (shown in green). Cells were imaged on a Zeiss LSM 510 confocal microscope. Serial optical sections collected at 0.35 μm intervals were used to create maximum projection images. Quantification was performed analyzing the fluorescence intensity of 3-4 independent areas per neuron using MetaMorph 6.0 software (Universal Imaging Corp) and is presented as ratio surface/intracellular intensities (mean ±SEM).

Generation of Neuronal Membrane Fractions

The crude membrane fraction was generated as previously described (Sanz-Clemente, et. al. 2010). Briefly, cortical neurons were harvested in PBS containing 0.1 mM $CaCl_2$ and 1 mM $MgCl_2$, and pelleted by centrifugation. Pellets were resuspended in hypotonic buffer (10 mM Tris, 1 mM $NaVO_4$) and sonicated. Membranes were isolated by centrifugation and resuspended in SDS loading buffer. Samples were then run on SDS-PAGE and immunoblotted with the indicated antibodies. For phosphorylation state specific and total immunoblots, the same membrane was used following antibody stripping

Subcellular Fractionation of Neurons

Biochemical subcellular fraction followed established protocols. Briefly, brain tissue or cells were homogenized in homogenization buffer (0.32M HEPES-buffered sucrose) containing protease (ROCHE) and phosphatase (Sigma) inhibitors and centrifuged for 10 min at 1,000 g to remove nuclei and large debris. The supernatant was centrifuged at 10,000 g for 15 min to generate

the synaptosomal fraction (P2). P2 was resuspended in hypotonic buffer, sonicated, and centrifuged at 25,000 g to generate the SPM fraction (P3). To isolate PSDs, SPMs were resuspended in PBS containing 1% Triton X-100 and ultracentrifuged at 100,000 g for 1 hour. Pellets containing the PSD were resuspended in PBS.

Inmmunoprecipitation

SPM fraction was obtained from rat brain cortex as explained before, dissolved in PBS 1% TX-100 and ultracentrifuged at 100,000 g for 1 hour. Pellet (PSD) was discarded, and the "extrasynaptic membranes" fraction (SN) was incubated with 2µg GluN2B antibody (or IgG as a control) for 1 hour at 4ºC with rotation. BSA-preblocked protein A-Sepharose beads were added to the lysate and incubated for 1 additional hour. After 3x10 minutes washes with cold PBS 1% TX-100, samples were immunoblotted with the indicated antibodies.

Total Internal Reflection Fluorescence Microscopy

Hippocampal cells were plated in glass bottom dishes (Matek). On DIV 10, cells were cotransfected with the indicated constructs. Cells were imaged in DIV 14 on a NIKON X1 spinning disk confocal microscope. During imaging, cells were maintained at 37°C with appropriate humidity and gas using a Tokai Hit incubation chamber. Timelapse images establishing baseline and following drug response were acquired with NIKON elements software and analyzed using FIJI. Changes in intensity from baseline are reported as mean ± SEM.

Acknowledgments

We thank Luca Zangrandi for his technical assistance. We also thank the Northwestern Center for Advanced Microscopy for their assistance in planning and analyzing imaging experiments. This research was supported by NIGMS (T32GM008061) (A.M.C.), NIMH (K08MH100562) (JAG) and NIA (K99AG041225) and a NARSAD Young Investigator Grant from the Brain & Behavior Research Foundation (#24133) (A.S.-C.).

References

Chen, B.S., Gray, J.A., Sanz-Clemente, A., Wei, Z., Thomas, E.V., Nicoll, R.A., and Roche, K.W. (2012). SAP102 mediates synaptic clearance of NMDA receptors. Cell reports *2*, 1120-1128.

Chung, H.J., Huang, Y.H., Lau, L.F., and Huganir, R.L. (2004). Regulation of the NMDA receptor complex and trafficking by activity-dependent phosphorylation of the NR2B subunit PDZ ligand. The Journal of neuroscience : the official journal of the Society for Neuroscience *24*, 10248-10259.

Cohen, P.T. (2002). Protein phosphatase 1--targeted in many directions. J Cell Sci *115*, 241-256.
Dore, K., Stein, I.S., Brock, J.A., Castillo, P.E., Zito, K., and Sjostrom, P.J. (2017).

Unconventional NMDA Receptor Signaling. The Journal of neuroscience : the official journal of the Society for Neuroscience *37*, 10800-10807.

Dupuis, J.P., Ladepeche, L., Seth, H., Bard, L., Varela, J., Mikasova, L., Bouchet, D., Rogemond, V., Honnorat, J., Hanse, E.*, et al.* (2014). Surface dynamics of GluN2B-NMDA receptors controls plasticity of maturing glutamate synapses. The EMBO journal *33*, 842-861.
Eto, M., and Brautigan, D.L. (2012). Endogenous inhibitor proteins that connect Ser/Thr kinases and phosphatases in cell signaling. IUBMB Life *64*, 732-739.

Glausier, J.R., Maddox, M., Hemmings, H.C., Jr., Nairn, A.C., Greengard, P., and Muly, E.C. (2010). Localization of dopamine- and cAMP-regulated phosphoprotein-32 and inhibitor-1 in area 9 of Macaca mulatta prefrontal cortex. Neuroscience *167*, 428-438.

Hardingham, G.E., Fukunaga, Y., and Bading, H. (2002). Extrasynaptic NMDARs oppose synaptic NMDARs by triggering CREB shut-off and cell death pathways. Nat Neurosci *5*, 405-414.

Harney, S.C., Jane, D.E., and Anwyl, R. (2008). Extrasynaptic NR2D-containing NMDARs are recruited to the synapse during LTP of NMDAR-EPSCs. The Journal of neuroscience : the official journal of the Society for Neuroscience *28*, 11685-11694.

Hendrickx, A., Beullens, M., Ceulemans, H., Den Abt, T., Van Eynde, A., Nicolaescu, E., Lesage, B., and Bollen, M. (2009). Docking motif-guided mapping of the interactome of protein phosphatase-1. Chem Biol *16*, 365-371.

Hou, H., Sun, L., Siddoway, B.A., Petralia, R.S., Yang, H., Gu, H., Nairn, A.C., and Xia, H. (2013). Synaptic NMDA receptor stimulation activates PP1 by inhibiting its phosphorylation by Cdk5. The Journal of cell biology *203*, 521-535.

Hunt, D.L., and Castillo, P.E. (2012). Synaptic plasticity of NMDA receptors: mechanisms and functional implications. Current opinion in neurobiology *22*, 496-508.

Hunt, D.L., Puente, N., Grandes, P., and Castillo, P.E. (2013). Bidirectional NMDA receptor plasticity controls CA3 output and heterosynaptic metaplasticity. Nature neuroscience *16*, 1049-1059.

Ishihara, H., Martin, B.L., Brautigan, D.L., Karaki, H., Ozaki, H., Kato, Y., Fusetani, N., Watabe, S., Hashimoto, K., Uemura, D.*, et al.* (1989). Calyculin A and okadaic acid: inhibitors of protein phosphatase activity. Biochem Biophys Res Commun *159*, 871-877.

Lavezzari, G., McCallum, J., Dewey, C.M., and Roche, K.W. (2004). Subunit-specific regulation of NMDA receptor endocytosis. The Journal of neuroscience : the official journal of the Society for Neuroscience *24*, 6383-6391.

Lussier, M.P., Sanz-Clemente, A., and Roche, K.W. (2015). Dynamic Regulation of N-Methyl-d-aspartate (NMDA) and alpha-Amino-3-hydroxy-5-methyl-4-isoxazolepropionic Acid (AMPA) Receptors by Posttranslational Modifications. The Journal of biological chemistry *290*, 28596-28603.

Merrill, M.A., Chen, Y., Strack, S., and Hell, J.W. (2005). Activity-driven postsynaptic translocation of CaMKII. Trends in pharmacological sciences *26*, 645-653.

Morishita, W., Connor, J.H., Xia, H., Quinlan, E.M., Shenolikar, S., and Malenka, R.C. (2001). Regulation of synaptic strength by protein phosphatase 1. Neuron *32*, 1133-1148.

Paoletti, P., Bellone, C., and Zhou, Q. (2013). NMDA receptor subunit diversity: impact on receptor properties, synaptic plasticity and disease. Nature reviews Neuroscience *14*, 383-400.

Papouin, T., and Oliet, S.H. (2014). Organization, control and function of extrasynaptic NMDA receptors. Philosophical transactions of the Royal Society of London Series B, Biological sciences *369*, 20130601.

Parsons, M.P., and Raymond, L.A. (2014). Extrasynaptic NMDA receptor involvement in central nervous system disorders. Neuron *82*, 279-293.

Sanz-Clemente, A., Gray, J.A., Ogilvie, K.A., Nicoll, R.A., and Roche, K.W. (2013a). Activated CaMKII couples GluN2B and casein kinase 2 to control synaptic NMDA receptors. Cell reports *3*, 607-614.

Sanz-Clemente, A., Matta, J.A., Isaac, J.T., and Roche, K.W. (2010). Casein kinase 2 regulates the NR2 subunit composition of synaptic NMDA receptors. Neuron *67*, 984-996.

Sanz-Clemente, A., Nicoll, R.A., and Roche, K.W. (2013b). Diversity in NMDA Receptor Composition: Many Regulators, Many Consequences. The Neuroscientist : a review journal bringing neurobiology, neurology and psychiatry *19*, 62-75.

Siddoway, B., Hou, H., and Xia, H. (2014). Molecular mechanisms of homeostatic synaptic downscaling. Neuropharmacology *78*, 38-44.

Siddoway, B.A., Altimimi, H.F., Hou, H., Petralia, R.S., Xu, B., Stellwagen, D., and Xia, H. (2013). An essential role for inhibitor-2 regulation of protein phosphatase-1 in synaptic scaling. The Journal of neuroscience : the official journal of the Society for Neuroscience *33*, 11206-11211.

Strack, S., Kini, S., Ebner, F.F., Wadzinski, B.E., and Colbran, R.J. (1999). Differential cellular and subcellular localization of protein phosphatase 1 isoforms in brain. The Journal of comparative neurology *413*, 373-384.

Szatmari, E., Habas, A., Yang, P., Zheng, J.J., Hagg, T., and Hetman, M. (2005). A positive feedback loop between glycogen synthase kinase 3beta and protein phosphatase 1 after stimulation of NR2B NMDA receptors in forebrain neurons. The Journal of biological chemistry *280*, 37526-37535.

Tovar, K.R., and Westbrook, G.L. (2002). Mobile NMDA receptors at hippocampal synapses. Neuron *34*, 255-264.

Virshup, D.M., and Shenolikar, S. (2009). From promiscuity to precision: protein phosphatases get a makeover. Mol Cell *33*, 537-545.

Woolfrey, K.M., and Dell'Acqua, M.L. (2015). Coordination of Protein Phosphorylation and Dephosphorylation in Synaptic Plasticity. The Journal of biological chemistry *290*, 28604-28612.

Zhang, J., Zhang, Z., Brew, K., and Lee, E.Y. (1996). Mutational analysis of the catalytic subunit of muscle protein phosphatase-1. Biochemistry *35*, 6276-6282.

FIGURE LEGENDS

FIGURE 1: Phosphorylation of the PDZ-ligand of the GluN2B subunit (GluN2B-pS1480) of NMDARs maintains NMDAR segregated at extrasynaptic membranes.

A) Hippocampal neurons were transfected at DIV7 with GFP-GluN2B WT or the phospho-mimetic mutant S1480E. At DIV13-14 recycling ratio (recycled/internalized) of the exogenous receptors was analyzed using an antibody-feeding approach (see Methods for details). Graph represents mean ± SEM. ns=non-significant in a one-way ANOVA test. N=3, n(WT, S1408E)=22,20.

B) Organotypic hippocampal slices were prepared from P7 *Grin2a*$^{fl/fl}$*Grin2b*$^{fl/fl}$ mice, biolistically transfected with either Cre or Cre + GluN2B-S1480E at DIV2-4, and paired whole-cell recordings were obtained by Cre-expressing and neighboring control CA1 pyramidal neurons at DIV18-24. Left, scatter plots of peak amplitudes of NMDAR-EPSCs from single pairs (open circles) and mean ± SEM (filled circles) from transfected and control cells. Dashed lines represent linear regression and 95% confidence interval. Sample traces: control cell, black; transfected cell, green/red; scale bars represent 100 ms and 100 pA. Right, bars represent the mean ± SEM of the ratios of transfected to control cells from each pair, expressed as percentages. Data were analyzed by the Mann-Whitney U test, $p = 0.536$.

C) After NMDAR-ESPC measurement, whole-cell responses to 100 µM NMDA puffed onto the same cells as in (B). Left, scatter plots of peak amplitudes of NMDA responses from single pairs (open circles) and mean ± SEM (filled circles) from transfected and control cells. Dashed lines represent linear regression and 95% confidence interval. Sample traces: control cell, black; transfected cell, green/red; scale bars represent 5 sec and 400 pA. Right, bars represent the mean ± SEM of the ratios of transfected to control cells from each pair, expressed as percentages. ***$p < 0.001$ using the Mann-Whitney U test.

FIGURE 2: Co-activation of synaptic and extrasynaptic NMDAR promotes Protein Phosphatase 1 (PP1)-mediated dephosphorylation of S1480 at surface-expressed GluN2B subunits.

Level of GluN2B-pS1480 in DIV21-28 cortical primary neurons after the indicated manipulations was analyzed by immunoblotting. Graphs represent mean ± SEM. Unless otherwise noted, *$p<.05$, **$p<.01$, ****$p<.0001$ using a one-way ANOVA test.

A) Biotinylation experiment in DIV24-28 cortical neurons after induction of GluN2B-pS1480 dephosphorylation by NMDA incubation (50 µM 10 min). M denotes marker. **$p<.01$ in a Mann-Whitney U test. N=5

B) Isolation of synaptic plasma membrane (SPM) fraction from DIV14-21 cortical neurons. Graph represents mean +/- SEM. *$p<.05$, **$p<.01$ in a Mann-Whitney U test. N=5

C) Synaptic (50 µM Bicuculline for 20 min), Extrasynaptic (50 µM NMDA for 10 min after blocking synaptic NMDARs by incubation with 50 µM Bicuculline in the presence of 10 µM MK-801 for 10 min) or Global (50 µM NMDA for 10 min) activation of NMDARs in DIV21-28 cortical neurons. N=3

D) Incubation with different phosphatase inhibitors for 45 min: Fostriecin for PP2A/4 (Fos, 1 μM), FK506 for PP2B (FK, 1 μM), Okadaic Acid for PP2A at 20 nM and PP2A/PP1 at 50 nM (OA, 20 or 50 nM), and Calyculin A for PP1/PP2A (Cal A, 100 nM). N=10

E) Preincubation of cortical neurons with 100 nM CalA for 45 min before induction of GluN2B-pS1480 dephosphorylation by bath application of NMDA (50 μM NMDA for 10 min).

F) Lentiviral transduction of the dominant negative form of GFP-PP1 alpha and gamma (PP1 D95N) and GFP (as a control) in cortical neurons for 10-14 days. GluN2B-pS1480 dephosphorylation was induced with NMDA as before. N=6

FIGURE 3: Regulation of the PP1-dependent dephosphorylation of GluN2B S1480.

All graphs represents mean ± SEM. Unless otherwise noted, ns=non-significant, *p<.05, **p<.01, ***p<.001, ****p<.0001 in a Mann-Whitney U test.

A) PP1 is regulated by 1) inhibitory CDK5 phosphorylation 2) complexing by endogenous inhibitor proteins or 3) targeting to a correct substrate.

B) Pharmacological activation of Inhibitor-2 (I-2) by blocking GSK3 (CHIR99021, 50 μM for 2 hours) blocks the NMDA-triggered dephosphorylation of GluN2B-pS1480. **p<.01 in a one-way ANOVA test. N=8

C) NMDA-induced translocation to the plasma membrane of GFP-PP1 and GFP-CaMKII (as a control) was evaluated by in DIV14 hippocampal cultures by Total Internal Reflection Fluorescence (TIRF) microscopy. Baseline fluorescence was recorded for 5 mins prior to the addition of NMDA as before. Graph represents increase in TIRF fluorescence over time. N=11.

D) The synaptic plasma membrane (SPM) fraction of DIV14-21 cortical neurons was isolated and the presence of the indicated proteins evaluated by immunoblotting. Protein levels were normalized to transferrin receptor (Tfr) in each condition and then normalized to control surface expression level. N=4

E) Extrasynaptic fraction from rat cortex was isolated and the association of GluN2B, PP1 and I-2 was analyzed by co-immunoprecipitation with anti-GluN2B antibody.

F) GluN2B-pS1480 dephosphorylation was induced in cortical neurons of the indicated DIV by incubating with 50 μM NMDA for 10 min as before. N=5

G) Level of PP1 present in the SPM fraction of mice of the indicated age was assessed by immunoblotting. ***p<.001 in a one-way ANOVA test. N=8

FIGURE 4: PP1 activity modulates NMDAR synaptic localization.

All graphs represents mean ± SEM. *p<.05, **p<.01, ***p<.001 in a Mann-Whitney U test.

A) Global synaptic and extrasynaptic NMDAR activation triggers PP1 activity to promote dephosphorylation of GluN2B which modulates its synaptic content.

B) DIV18-21 cortical neurons were pre-treated with OA (50 nM for 45 min) or NMDA (50 μM for 10 min) and synaptic NMDAR stimulation performed by incubating with 20 uM Bicuculline and 100 μM 4-AP for 30 min. Levels of ERK and phosphoERK evaluated by immunoblotting. N=7

C) Structured Illumination Microscopy (SIM) super-resolution micrographs were acquired. To quantify the synaptic expression of exogenous receptor, Nikon NIS elements software identifies colocalized nano-objects (containing GFP-GluN2B (red) and endogenous PSD-95

(blue), and pseudocolored white) and presents counts of colocalized vs total GluN2B nanobjects.

D) Primary hippocampal neurons were transfected with GFP-GluN2B and treated with OA or NMDA as before. Structured Illumination Microscopy (SIM) super-resolution micrographs were acquired and counts of colocalized GluN2B nano-objects were obtained and normalized to total GluN2B nano-objects. N=4

E) Postsynaptic Density (PSD) fraction was isolated from acute hippocampal slices from P70-96 mice treated with NMDA (50 µM for 10 min) or Cal A (100 nM for 30 min to 1 hour) to promote or inhibit GluN2B-pS1480 dephosphorylation. Levels of GluN2B-pS1480 and synaptic GluN2B were analyzed by immunoblotting and normalized to the synaptic marker homer. N=9,7 (Cal A,NMDA)

SUPPLEMENTARY FIGURE LEGENDS

FIGURE S1: Validation of custom generated antibody against GluN2B-pS1480.

A) DIV14 cortical neurons were treated with AP5 (100 µM, overnight), TTX (40 µM, overnight), Bicuculline (40 µM, 8 hours), or KCl (20 mM, 5 min).

B) Crude membrane fractions from DIV14 cortical neurons were incubated in the presence of Antarctic phosphatase for 1 hour.

FIGURE S2: Inhibitor-1 is not a crucial regulator of PP1-mediated GluN2B dephosphorylation.

Cortical primary neurons or tissue was analyzed by immunoblotting following the indicated manipulations. All graphs represents mean ± SEM. ns=non-significant, ***p<.001 using a one-way ANOVA test.

A) Acute hippocampal slices from P70 mice were treated with NMDA (50 µM, 15 min). N=2

B) DIV14 cortical neurons were treated with either forsksolin (10 µM, 45 min) or H-89 (10 µM, 45 min). N=3

C) Preincubation of DIV14 cortical neurons with FK506 (1 µM, 45 min) before induction of GluN2B-pS1480 dephosphorylation by bath application of glutamate (100 µM, 10 min). N=8

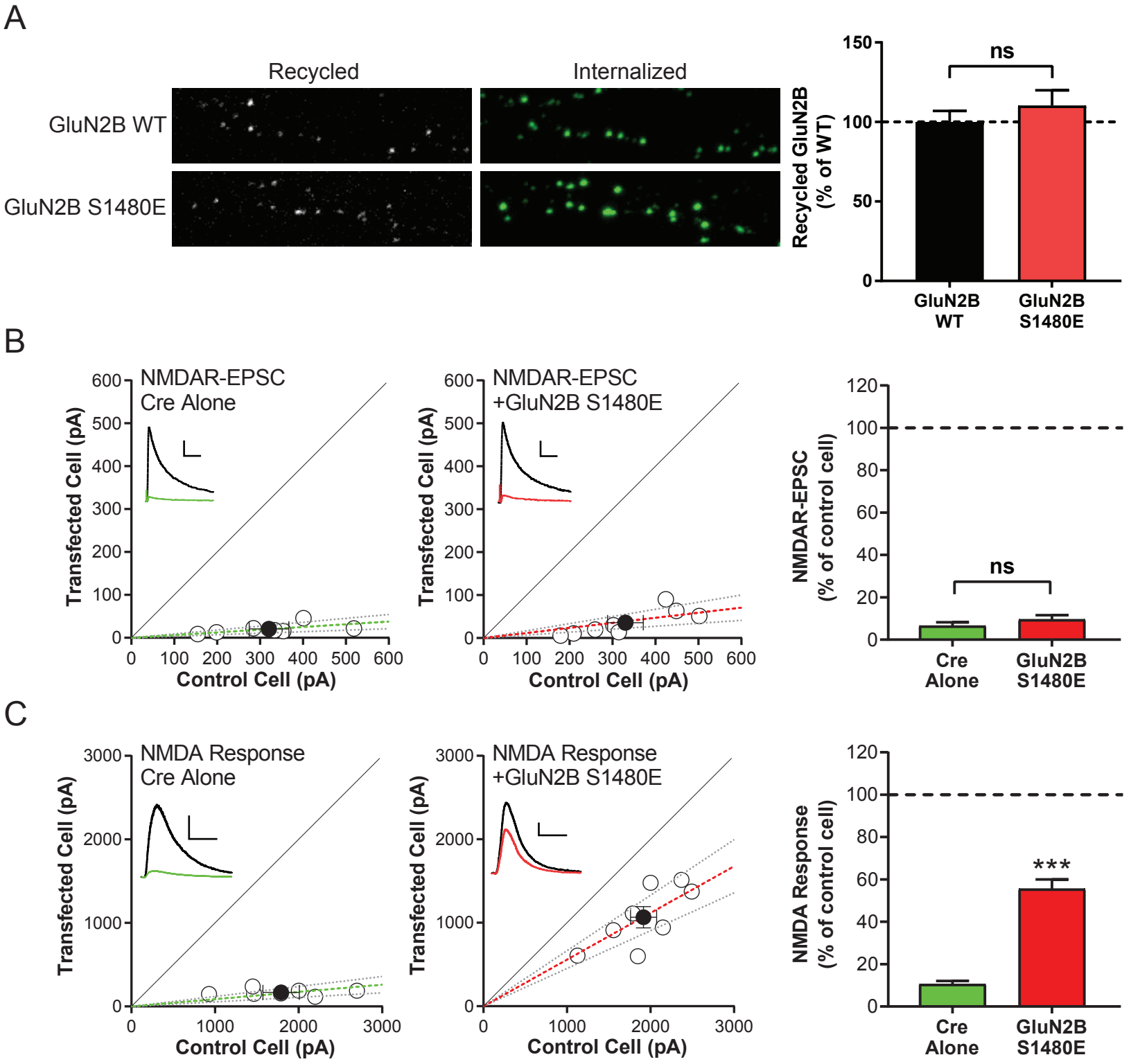
A
Recycled
Internalized
GluN2B WT
GluN2B S1480E
Recycled GluN2B (% of WT)
150
100
50
0
ns
GluN2B WT
GluN2B S1480E
B
NMDAR-EPSC
Cre Alone
NMDAR-EPSC
+GluN2B S1480E
Transfected Cell (pA)
Control Cell (pA)
0
100
200
300
400
500
600
NMDAR-EPSC (% of control cell)
120
80
60
40
20
ns
Cre Alone
GluN2B S1480E
C
NMDA Response
Cre Alone
NMDA Response
+GluN2B S1480E
Transfected Cell (pA)
Control Cell (pA)
0
1000
2000
3000
NMDA Response (% of control cell)
***
Cre Alone
GluN2B S1480E

Figure 1

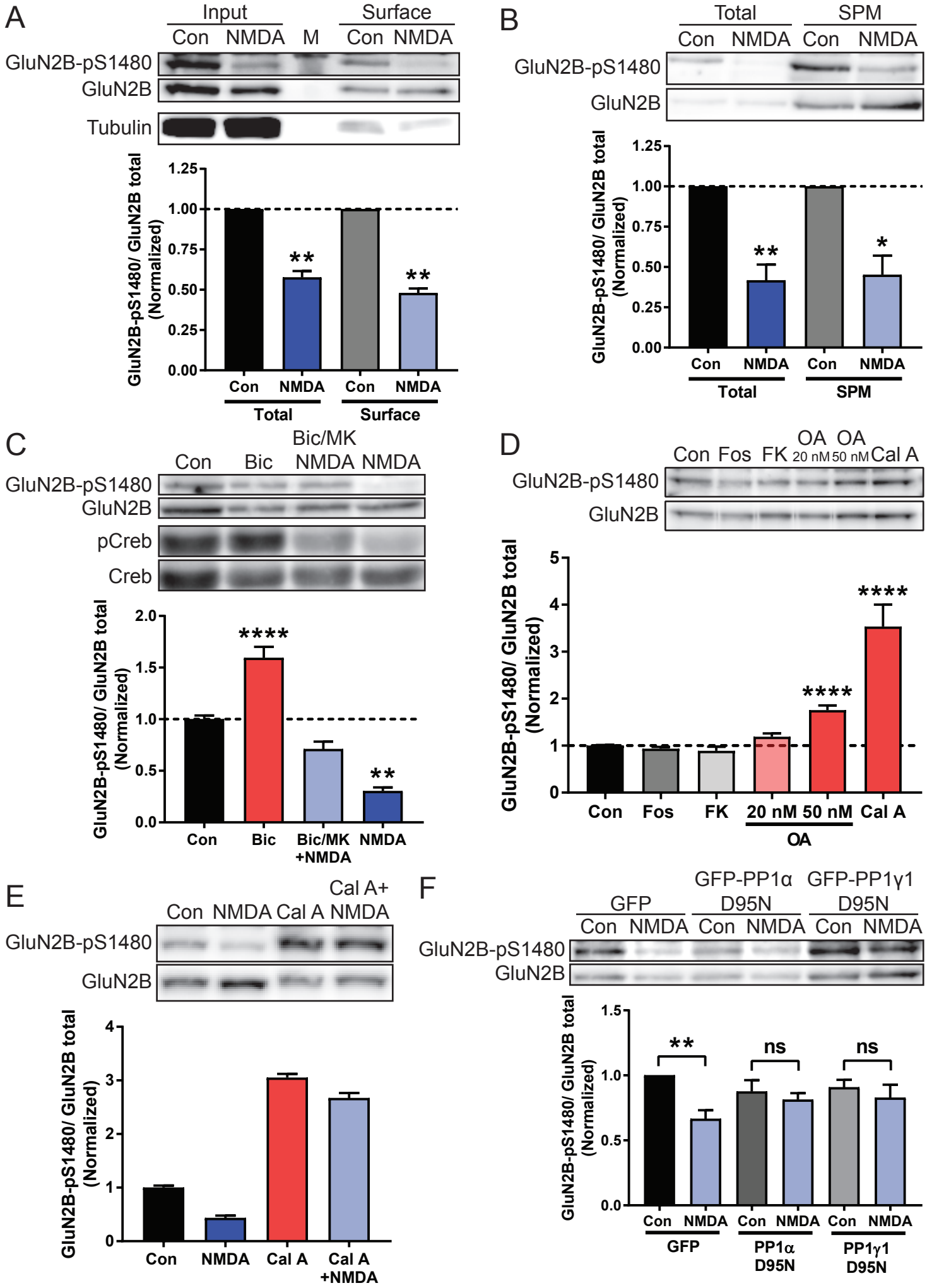
A
Input
Surface
Con NMDA M Con NMDA
GluN2B-pS1480
GluN2B
Tubulin
GluN2B-pS1480/ GluN2B total (Normalized)
1.25
1.00
0.75
0.50
0.25
0.00
**
**
Con NMDA Con NMDA
Total
Surface
B
Total
SPM
Con NMDA Con NMDA
GluN2B-pS1480
GluN2B
GluN2B-pS1480/ GluN2B total (Normalized)
1.25
1.00
0.75
0.50
0.25
0.00
**
*
Con NMDA Con NMDA
Total
SPM
C
Bic/MK
Con Bic NMDA NMDA
GluN2B-pS1480
GluN2B
pCreb
Creb
GluN2B-pS1480/ GluN2B total (Normalized)
2.0
1.5
1.0
0.5
0.0
****
**
Con Bic Bic/MK +NMDA NMDA
D
OA OA
Con Fos FK 20 nM 50 nM Cal A
GluN2B-pS1480
GluN2B
GluN2B-pS1480/ GluN2B total (Normalized)
5
4
3
2
1
0
****
****
Con Fos FK 20 nM 50 nM Cal A
OA
E
Cal A+
Con NMDA Cal A NMDA
GluN2B-pS1480
GluN2B
GluN2B-pS1480/ GluN2B total (Normalized)
4
3
2
1
0
Con NMDA Cal A Cal A +NMDA
F
GFP
GFP-PP1α D95N
GFP-PP1γ1 D95N
Con NMDA Con NMDA Con NMDA
GluN2B-pS1480
GluN2B
GluN2B-pS1480/ GluN2B total (Normalized)
1.5
1.0
0.5
0.0
**
ns
ns
Con NMDA Con NMDA Con NMDA
GFP
PP1α D95N
PP1γ1 D95N

Figure 2

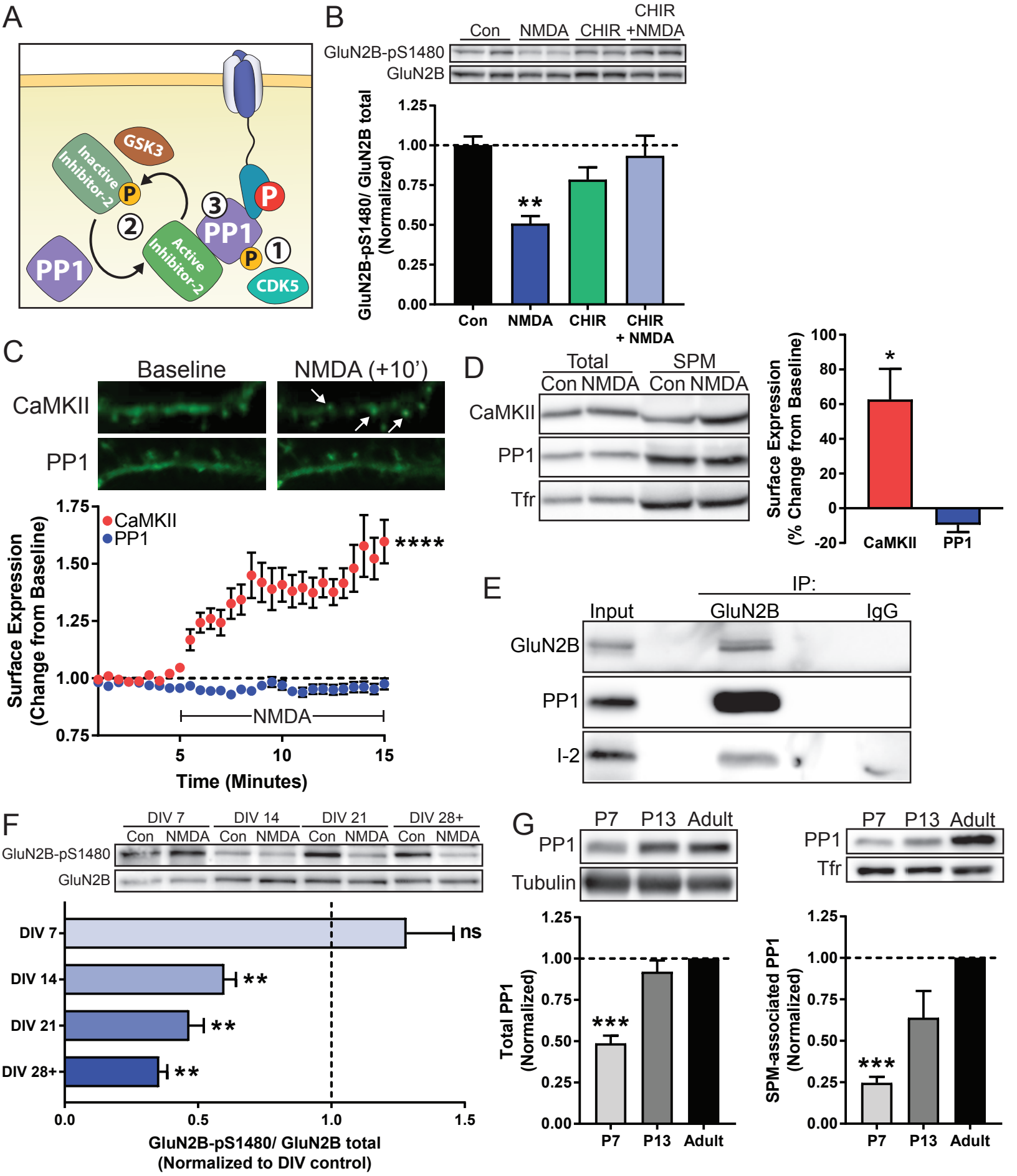
A
GSK3
Inactive Inhibitor-2
P
PP1
Active Inhibitor-2
CDK5
B
Con
NMDA
CHIR
CHIR +NMDA
GluN2B-pS1480
GluN2B
GluN2B-pS1480/ GluN2B total (Normalized)
Con
NMDA
CHIR
CHIR + NMDA
C
Baseline
NMDA (+10')
CaMKII
PP1
Surface Expression (Change from Baseline)
Time (Minutes)
NMDA
D
Total
SPM
Con NMDA Con NMDA
CaMKII
PP1
Tfr
Surface Expression (% Change from Baseline)
E
IP:
Input
GluN2B
IgG
GluN2B
PP1
I-2
F
DIV 7
DIV 14
DIV 21
DIV 28+
Con NMDA Con NMDA Con NMDA Con NMDA
GluN2B-pS1480
GluN2B
ns
GluN2B-pS1480/ GluN2B total (Normalized to DIV control)
G
P7 P13 Adult
PP1
Tubulin
Tfr
Total PP1 (Normalized)
SPM-associated PP1 (Normalized)

Figure 3

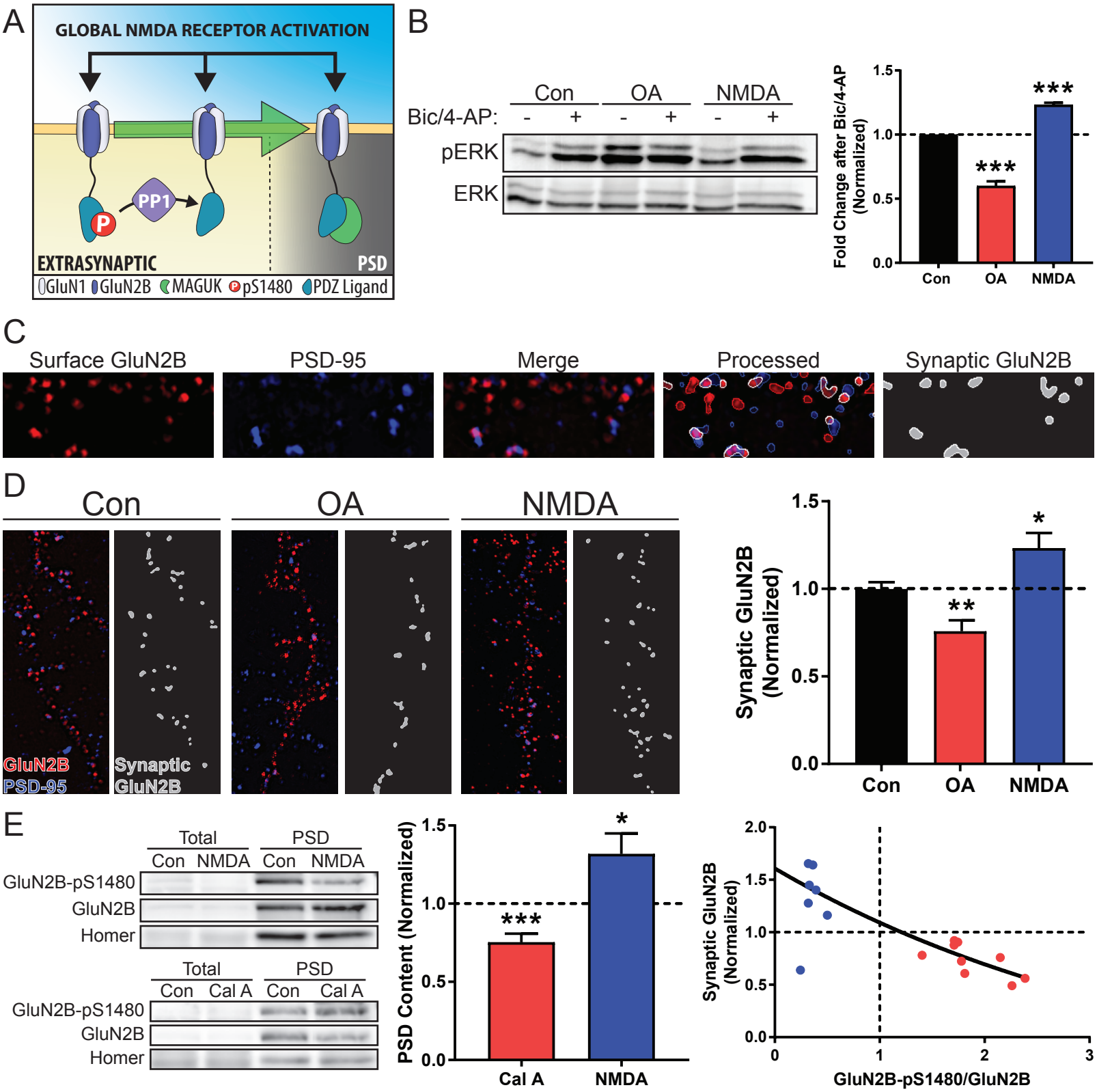
A
GLOBAL NMDA RECEPTOR ACTIVATION
PP1
P
EXTRASYNAPTIC
PSD
GluN1 GluN2B MAGUK pS1480 PDZ Ligand
B
Con
OA
NMDA
Bic/4-AP: - + - + - +
pERK
ERK
Fold Change after Bic/4-AP (Normalized)
1.5
1.0
0.5
0.0
***
***
Con
OA
NMDA
C
Surface GluN2B
PSD-95
Merge
Processed
Synaptic GluN2B
D
Con
OA
NMDA
GluN2B
PSD-95
Synaptic GluN2B
Synaptic GluN2B (Normalized)
1.5
1.0
0.5
0.0
*
**
Con
OA
NMDA
E
Total
PSD
Con NMDA Con NMDA
GluN2B-pS1480
GluN2B
Homer
Total
PSD
Con Cal A Con Cal A
GluN2B-pS1480
GluN2B
Homer
PSD Content (Normalized)
1.5
1.0
0.5
0.0
*
***
Cal A
NMDA
Synaptic GluN2B (Normalized)
2.0
1.5
1.0
0.5
0.0
0
1
2
3
GluN2B-pS1480/GluN2B

Figure 4

A

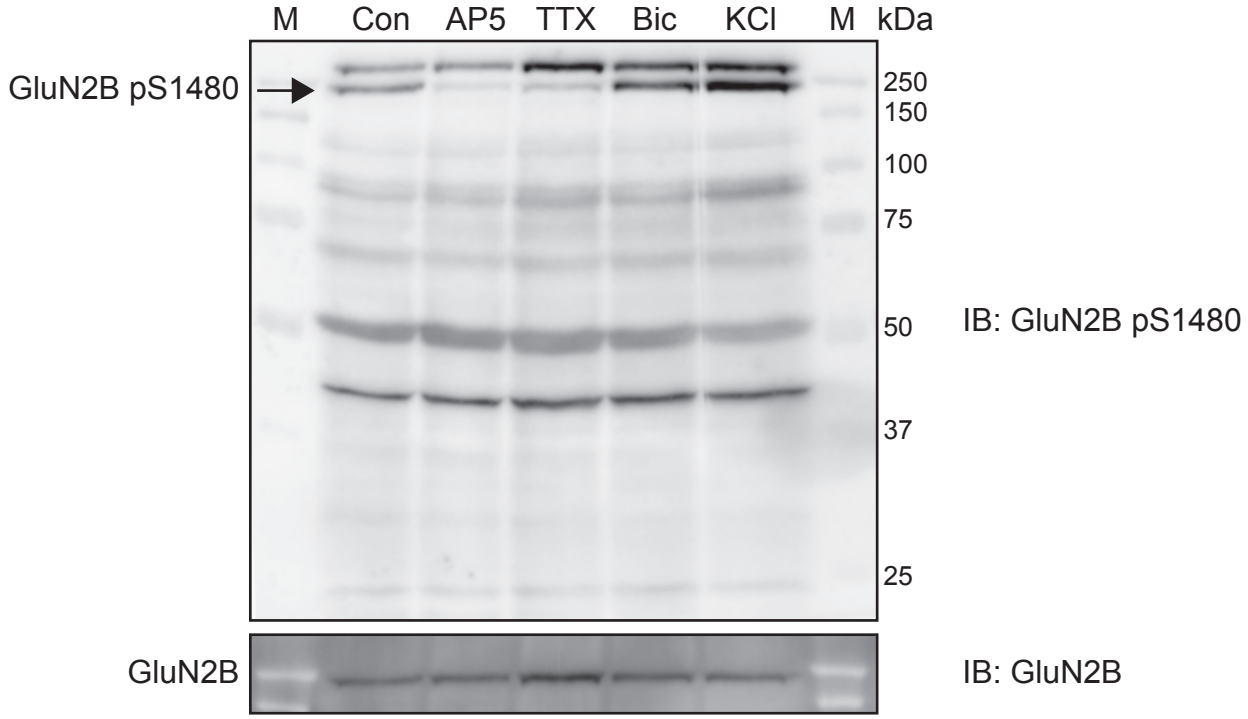
M
Con
AP5
TTX
Bic
KCl
M
kDa
GluN2B pS1480
250
150
100
75
50
37
25
IB: GluN2B pS1480
GluN2B
IB: GluN2B

B

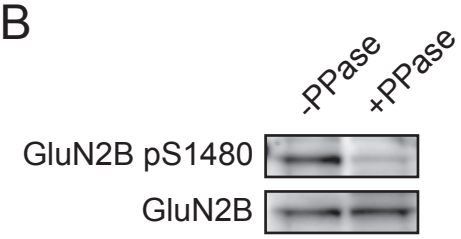
-PPase
+PPase
GluN2B pS1480
GluN2B

Figure S1

A

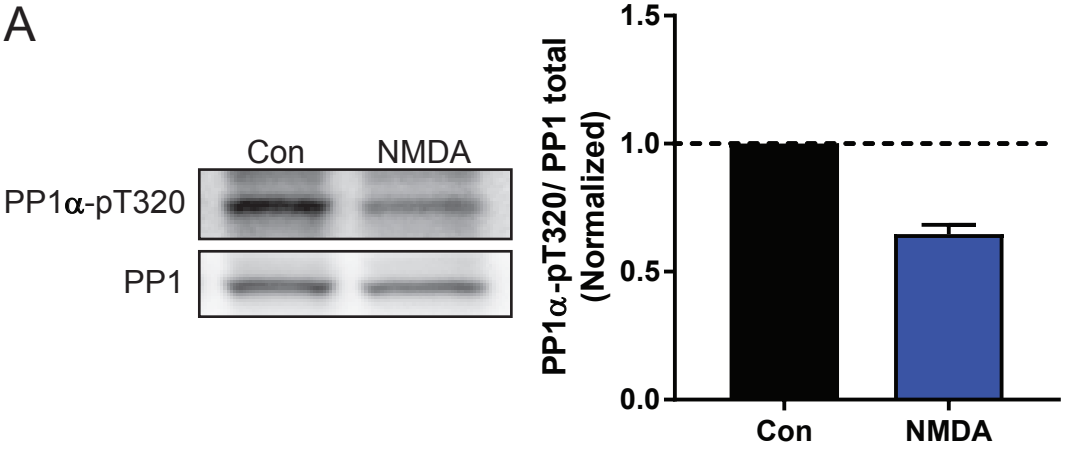

B

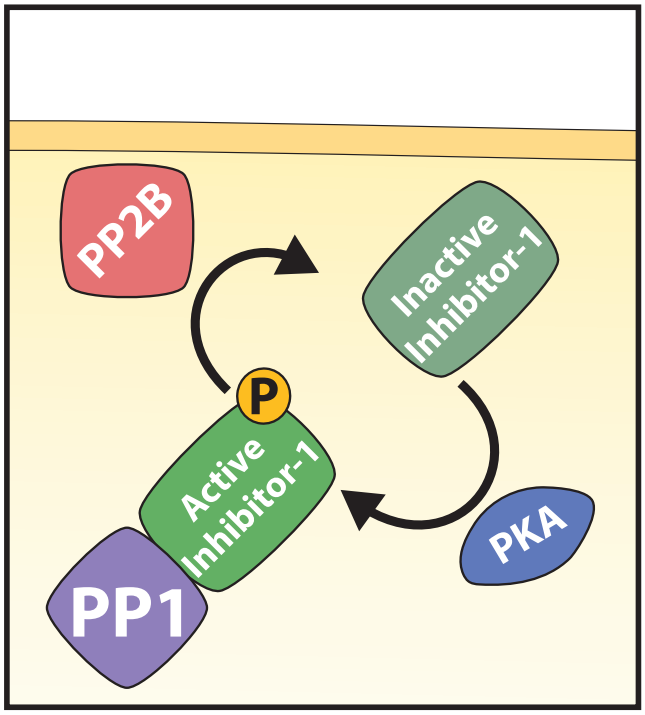

C

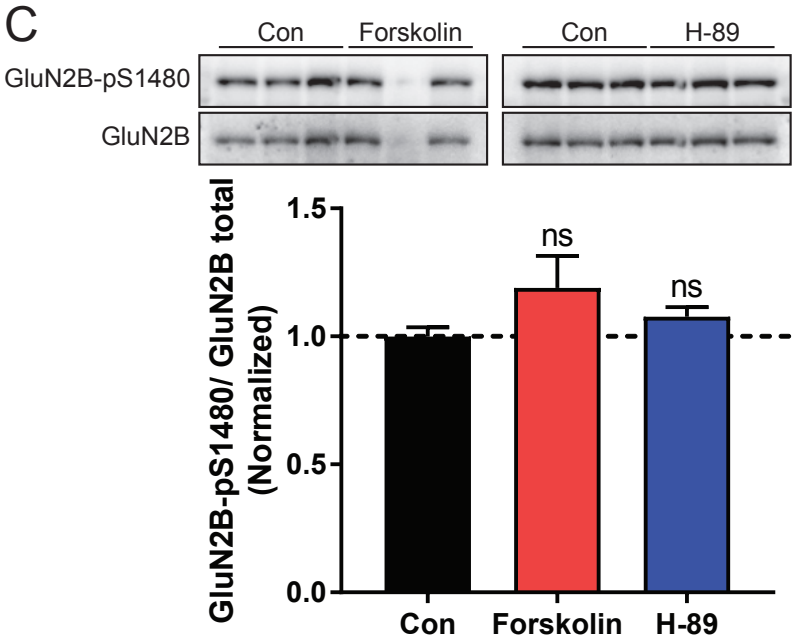

D

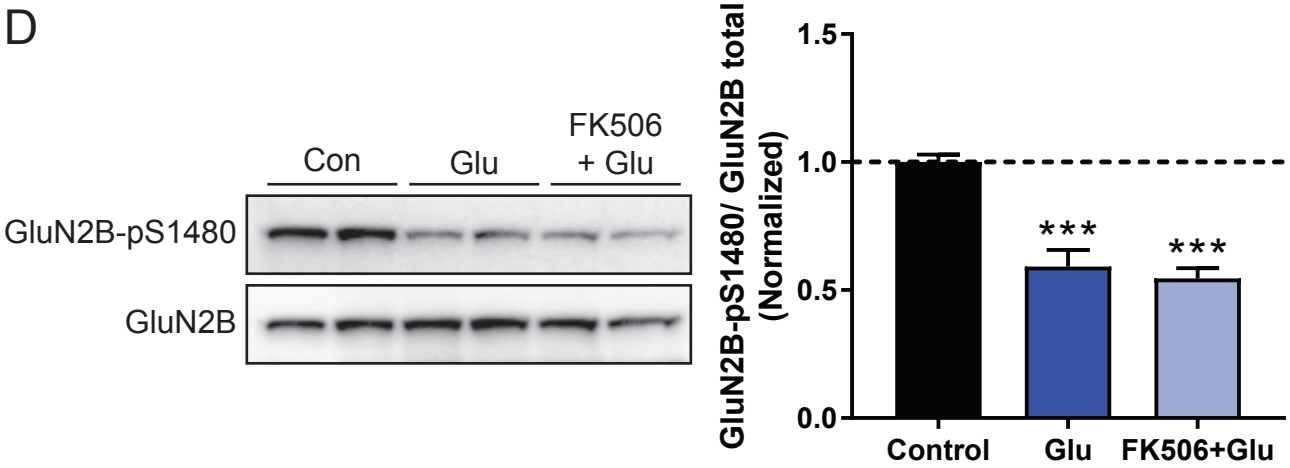

Figure S2